Journal of Aerosol Science 156 (2021) 105781

Contents lists available at ScienceDirect

Journal of Aerosol Science

journal homepage: http://www.elsevier.com/locate/jaerosci

Effects of renewable fuel and exhaust aftertreatment on primary and secondary emissions from a modern heavy-duty diesel engine

Louise Gren [a,b], Vilhelm B. Malmborg [a,b], John Falk [c], Lassi Markula [d], Maja Novakovic [e], Sam Shamun [e], Axel C. Eriksson [a,b,c], Thomas B. Kristensen [c], Birgitta Svenningsson [c], Martin Tunér [e], Panu Karjalainen [a,d], Joakim Pagels [a,b,*]

[a] Ergonomics and Aerosol Technology, Lund University, Lund, SE-22100, Sweden
[b] NanoLund, Lund University, Lund, SE-22100, Sweden
[c] Division of Nuclear Physics, Lund University, Lund, SE-22100, Sweden
[d] Aerosol Physics Laboratory, Physics Unit, Tampere University, Tampere, FI-33014, Finland
[e] Division of Combustion Engines, Lund University, Lund, SE-22100, Sweden

ARTICLE INFO

Keywords:
Biodiesel
Renewable diesel
Secondary aerosol formation
Diesel oxidation catalyst
Diesel particulate filter
Diesel exhaust
Aerosol

ABSTRACT

Compared to petroleum diesel, renewable diesel fuels and exhaust aftertreatment systems can reduce primary exhaust emissions that are hazardous to human health and the environment. Secondary aerosol emissions which form upon atmospheric processing have, however, been less studied. This study aimed to quantify the impacts of replacing petroleum diesel with renewable fuels (hydrotreated vegetable oil [HVO] and rapeseed methyl ester [RME]) on primary and secondary aerosol emissions from a heavy-duty diesel engine at different stages of an exhaust aftertreatment system. Emission characterization was obtained by combining a battery of physical characterization techniques with chemical characterization using aerosol mass spectrometry.

At engine-out measurements, RME and HVO reduced primary particulate matter (PM) emissions (for example equivalent black carbon [eBC]) and secondary aerosol production (studied with an oxidation flow reactor [OFR]) by mass compared to petroleum diesel. The diesel oxidation catalyst (DOC) reduced primary nucleation mode emissions, reduced the effective density of soot mode emissions, and reduced secondary particle production by mass. The DOC + a diesel particulate filter removed >99% of the particle number and eBC emissions.

Volatile PM emissions (for example organic aerosol) were found to be distributed between the nucleation mode and soot mode for both primary and secondary emissions, to a degree that depends on both fuel type and aftertreatment. A high mass concentration of condensable species and a low condensation sink in the soot mode led to increased fractions of condensable species present in the nucleation mode. Aging in the OFR led to increases in particle effective density. Motoring the engine (running without combustion) showed that the nucleation mode originated primarily from lubricating oil, and nonvolatile nanoparticle emissions were identified down to 1.2 nm in particle size.

In conclusion, replacing petroleum diesel with HVO and RME changes emission characteristics and can help reduce key aerosol emissions of relevance for adverse health and climate impact, especially for diesel engines with no or limited exhaust aftertreatment.

* Corresponding author. Ergonomics and Aerosol Technology, Lund University, Lund, SE-22100, Sweden.
E-mail address: joakim.pagels@design.lth.se (J. Pagels).

https://doi.org/10.1016/j.jaerosci.2021.105781
Received 30 November 2020; Received in revised form 11 February 2021; Accepted 24 February 2021
Available online 10 March 2021

1. Introduction

Vehicle emission legislation has become increasingly stringent in the past 20 years in order to combat air pollution and reduce carbon dioxide (CO_2) emissions. Emission legislation and sustainability goals have forced the development and implementation of various emission controls, such as more efficient engines with lower emissions, exhaust aftertreatment systems (EATSs) and renewable diesel fuels to reduce the emissions. Primary emissions and the subsequent secondary organic aerosol (SOA) formation from combustion engines contribute considerably to urban and regional particulate air pollution (Gentner et al., 2017; Hallquist et al., 2009; Robinson et al., 2007). In this study, we investigate the effects of renewable diesel fuels and EATSs on the primary and secondary aerosol emissions of a heavy-duty diesel engine.

Emissions of untreated diesel exhaust (engine-out) are composed of major gas-phase species such as CO_2, carbon monoxide (CO), nitrogen oxides (NO_x), a complex mixture of gaseous hydrocarbons (HC), and of particulate matter (Matti Maricq, 2007). The particulate emissions from diesel engines are often characterized by a bimodal particle size distribution, with nucleation mode particles dominating the number concentration and soot mode particles dominating the total emitted mass (Burtscher, 2005; Matti Maricq, 2007). The soot mode consists of agglomerates of insoluble primary soot particles, primarily made up of elemental carbon (EC) arranged in graphitic-like material, with a varying degree of adsorbed or condensed volatile organic and inorganic matter on the surfaces (Kittelson, 1998; Matti Maricq, 2007). Early in the combustion process the soot matures to refractory black carbon (rBC). The concentration of eBC in the exhaust after the engine is often controlled by late cycle in-cylinder oxidation processes (Malmborg et al., 2017). Nucleation mode particles can be emitted as delayed primary emissions which form rapidly after cooling and dilution of the exhaust gas in the atmosphere in a sulfur-driven nucleation process (Karjalainen et al., 2014; Rönkkö et al., 2013). However, nanoparticle emissions have also been found in primary emissions at high temperatures and may contain nonvolatile cores (nanoclusters) that can later act as additional condensation sinks for gas-phase species to condense on in the dilution process (Karjalainen, Ntziachristos, et al., 2016; Kuuluvainen et al., 2020). Karjalainen, Timonen, et al. (2016) found that the nucleation particles originated from the lubricating oil, and that the nonvolatile core was composed of heavy organic or organometallic material. A recent paper by Kuuluvainen et al. (2020) proposed that nucleation cores in heavy-duty non-road engine exhaust can be divided into two independent particle modes where one is lubricant originated and the other is fuel originated. However, only the emissions before any aftertreatment (engine-out) were measured. When assessing atmospherically relevant emissions, the effect of EATSs on the nucleation mode particles are of vital importance.

The composition of the particulate fraction of diesel exhaust depends strongly on the combustion conditions and the type of fuel (Burtscher, 2005). Oxygenated renewable fuels, such as fatty acid methyl ester (FAME) fuels, can reduce particulate matter (PM), HC, and CO emissions, but may simultaneously lead to an increase in NO_x emissions (Knothe, Krahl, & Van Gerpen, 2015; Mahmudul et al., 2017; Matti Maricq, 2007). Exhaust PM from combustion with FAME fuels has been found to contain a higher organic carbon (Popovicheva et al., 2017) or soluble organic (Matti Maricq, 2007; Murtonen, Aakko-Saksa, Kuronen, Mikkonen, & Lehtoranta, 2010) mass fraction compared to diesel. FAME fuels can also impact the soot characteristics, and smaller primary particle and agglomerate sizes have been observed (Savic et al., 2016). Paraffinic renewable diesel fuels, such as hydrotreated vegetable oil (HVO), have in some studies been shown to reduce the PM, HC, CO, and NO_x emissions (Dimitriadis, Natsios, Dimaratos, & Katsaounis, 2018; Gren et al., 2020; Kuronen, Mikkonen, Aakko, & Murtonen, 2007; Murtonen et al., 2010) while other studies have shown negligible effects in comparison to petroleum diesel (Mizushima, Kawano, Ishii, Takada, & Sato, 2014; Shukla et al., 2018). However, the PM reduction observed for combustion with HVO is generally smaller compared to the reduction observed with FAME fuels (Knothe et al., 2015; Na et al., 2015). The different characteristics of the exhaust from HVO and FAME fuels could as well have effects of the operation and efficiency of the EATS.

EATSs are designed to reduce multiple pollutants found in diesel exhaust (Reşitoğlu, Altinişik, & Keskin, 2015), and are often composed of a series of units that treat different combustion products in each step. A common approach is to utilize a combination of a diesel oxidation catalyst (DOC) to reduce gas phase HC and CO, a diesel particulate filter (DPF) to reduce PM, and a NO_x reduction unit (Reşitoğlu et al., 2015). The DOC also reduces the organic fraction of the exhaust PM (Liu, Eckerle, & Ottinger, 2018; Zeraati-Rezaei, Alam, Xu, Beddows, & Harrison, 2020). Internal combustion controls, such as exhaust gas recirculation (EGR), are an alternative to reduce NO_x levels (Sorathia et al., 2012; Zheng, Reader, & Hawley, 2004), but at the expense of increased PM emissions (Gren et al., 2020). While the knowledge of primary emissions from renewable fuels is increasing, research is still needed on the impact of EATSs in combination with renewable fuels and the subsequent aging in the atmosphere.

Gas-phase emissions from diesel exhaust can be oxidized in the atmosphere to form secondary PM (Gentner et al., 2017; Schauer, Fraser, Cass, & Simoneit, 2002). Diesel exhaust is an important secondary organic aerosol (SOA) precursor and source of photochemical smog. SOA from diesel exhaust and other anthropogenic sources has also been found to have a higher oxidative potential compared to such sources' primary organic aerosols, and thus a potentially higher toxic potential (Pourkhesalian et al., 2015; J.; Zhou et al., 2019). While renewable diesel fuels generally reduce the primary PM emissions, the effect on SOA yields is less known, and similar SOA yields have been found for HVO (Karjalainen et al., 2019) and FAME type fuels (Gordon et al., 2014; Jathar et al., 2017; Watne et al., 2018) relative to petroleum diesel.

Many renewable fuels have a negligible or low aromatic content compared to petroleum diesel, which has been identified as a factor that could potentially reduce the SOA formation (Gentner et al., 2017). However, as the semi-volatile organic fraction of emissions from renewable oxygen-containing fuels (FAME fuels) can be higher compared to petroleum diesel (Matti Maricq, 2007; Murtonen et al., 2010; Popovicheva et al., 2017; Surawski et al., 2011), this may instead contribute to increasing the SOA formation potential per mass and possibly also to increasing the oxidative potential (Pourkhesalian et al., 2014, 2015). In addition, the role of

lubricating oil components on SOA formation remains unclear, but has been suggested to influence the SOA formation more strongly than the fuel composition (Karjalainen et al., 2019; Le Breton et al., 2019). EATSs, composed of units such as DOCs and DPFs, significantly decrease the secondary aerosol formation of both diesel and HVO (Karjalainen et al., 2019). While the use of renewable fuels and EATSs is increasing, reliable quantitative estimates of the impact on SOA formation remains uncertain (Gentner et al., 2017).

The aim of this study was to investigate the effects of an aftertreatment system and renewable diesel fuels on primary and secondary emissions. The exhaust emissions were measured: 1) before any aftertreatment system (engine-out), 2) after a diesel oxidation catalyst (DOC) alone, and 3) after a DOC and diesel particulate filter (DPF) in series. The fuels used were Swedish MK1 ultra-low sulfur diesel and two renewable diesel fuels: HVO, and a FAME fuel (rapeseed methyl ester [RME]).

2. Method

2.1. Engine operation, fuels and exhaust aftertreatment system

The experiments were performed during steady-state operating conditions of a modern heavy-duty diesel engine modified to operate on one active cylinder (original version 6-cylinder, 13-liter engine). A version similar to the test engine is offered on the market, using the same engine hardware for diesel fuel, HVO and RME-100. The test engine was equipped with an adjustable and cooled EGR system. A low amount of EGR was used that corresponded to a combustion cylinder intake O_2 concentration of 18%. Throughout the experiments, the engine was operated at a constant low load (6 bar gross indicated mean effective pressure, $IMEP_G$) and a speed of 1200 rpm. To simulate engine braking, the engine was additionally motored (without combustion) at the same speed (1200 rpm).

To allow a direct comparison between the emissions for the different fuels, the combustion phasing (CA50 position) was held constant at approximately 5 crank angle degrees (CAD) after the top dead center (ATDC). The effect of fine-tuning the start of injection (SOI) timing on CA50 was evaluated. Only minor differences were found and the same SOI was used for all fuels with only minor differences in injection duration. A CA50 at 5 CAD is near the optimum condition where maximum efficiency and reduced emissions can be achieved for the tested engine. An extra high-pressure injection common rail injection system supplied the fuel in a single injection at a pressure of 1200 bar through an injector with 10 holes and a 148° spray angle.

The fuels tested were Swedish MK1 ultra-low sulfur 100% petroleum diesel (B0, referred to as diesel), and two renewable diesel fuels: hydrotreated vegetable oil (HVO) and rapeseed methyl ester (RME). All fuels were tested without blending.

The EATS used was made up of two units: a diesel oxidation catalyst (DOC) and a diesel particulate filter (DPF) in a serial set-up with the DOC first. The two units were tailored for the single cylinder operation and this specific engine. The exhaust residence times inside the DOC and DPF can be considered similar to those in real vehicles. The DOC was a metallic catalyst (Pt:Pd) operating at the exhaust gas temperature, which was measured to 215 ± 6 °C for all fuels. The removal efficiency of HC and CO during the experiments confirmed that the DOC operated under adequate conditions. The DPF was a high porosity Cu–SiC model with a Pt catalyst. In modern commercial heavy-duty engines, NO_x reduction techniques, for example selective catalytic reduction (SCR) using urea, is often used together with a DOC and DPF. This type of device was not included in the study; however, it is worth mentioning that SCR catalysts have been found to emit excessive ammonia (NH_3) which caused new particle formation of non-volatile nucleation mode particles after the DPF in some studies (Amanatidis, Ntziachristos, Giechaskiel, Bergmann, & Samaras, 2014; Mamakos, Schwelberger, Fierz, & Giechaskiel, 2019), but not all (Karjalainen et al., 2019).

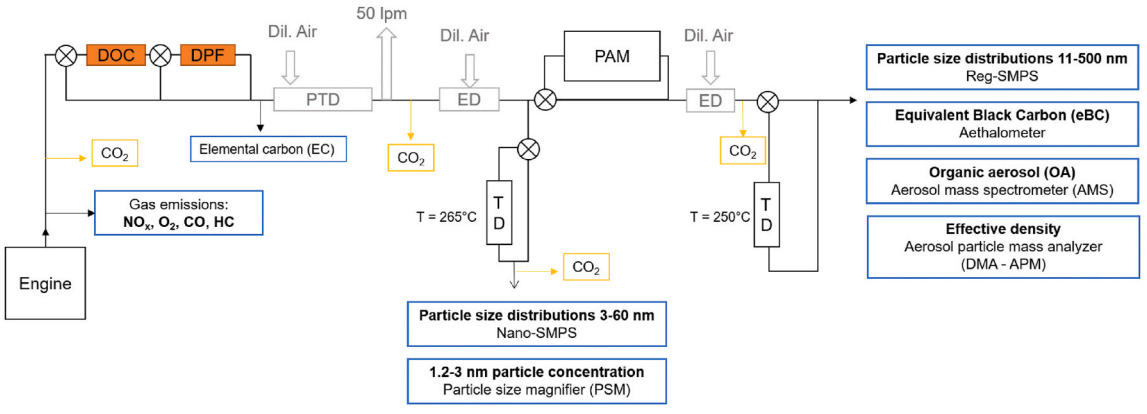

Fig. 1. The experimental setup. Sampling was carried out before the EATS (engine-out), after the diesel oxidation catalyst (DOC) or after the DOC in combination with the diesel particulate filter (DPF). Dilution was performed with a porous tube diluter (PTD) and two ejector diluters (ED). The exhaust was either analyzed: untreated (bypass), after simulated aging with the potential aerosol mass (PAM) chamber, or after heat treatment in the thermodenuders (TD).

2.1.1. Sampling setup and dilution strategy

The aerosol sampling was performed upstream (engine-out) and downstream of the different units of the EATS, that is, after the DOC or after the DOC + DPF. The measurement setup is shown in Fig. 1. The partial flow dilution setup was composed of a porous tube diluter (PTD) with a dilution ratio (DR) of 12 and a small residence time chamber (2.5 s), in order to stabilize the nucleation mode particles. A similar setup is described by Karjalainen et al. (2019). At the applied dilution conditions, the sampling system mimics atmospheric dilution in order to simulate a particle size distribution that can be expected to form under real-world driving conditions, especially with respect to particle formation by the nucleation of vapors (Ntziachristos et al., 2004; Rönkkö et al., 2006). After the PTD, the exhaust was further diluted with a Dekati ejector dilutor with a DR of 9. The nucleation mode particles were measured after these two dilution steps with a scanning mobility particle sizer (SMPS) operating in the size range 3–60 nm ('Nano-SMPS', DMA 3085 and CPC 3776, TSI Inc.), and a particle size magnifier ('PSM', A11 nCNC, cut sizes 1.2–3 nm, \Airmodus), with or without a thermodenuder that has low nanoparticle losses (Heikkilä et al., 2009) operated at 265 °C. In order to monitor the dilution ratios, CO_2 concentrations were measured with a non-dispersive infrared CO_2 analyzer (LI-8020, LI-COR Inc.) in every step of the dilution system.

Atmospheric aging was simulated using a potential aerosol mass (PAM) oxidation flow reactor (OFR) located downstream of the 2nd dilution step. Thermodenuder (Aerodyne Inc., at 250 °C) treatment and particle measurements were performed after a 3rd dilution step with a Dekati ejector diluter (DR 4–10). The particle number size distribution was measured with a regular SMPS (Reg-SMPS) operating in the size range of 11–500 nm (DMA 3082 and CPC 3772, TSI Inc.). The equivalent black carbon (eBC) concentration was measured using an aethalometer (AE33, Magee Scientific) from the attenuation at a wavelength of 880 nm (Drinovec et al., 2015). The particle effective density and mass-mobility relationship was measured with the DMA-APM method using an aerosol particle mass analyzer (APM 3600, Kanomax) in combination with a differential mobility analyzer (DMA model 3071, TSI Inc.) and a condensation particle counter (CPC Model 3075, TSI Inc.). The organic aerosol mass concentration and composition were measured with an aerosol mass spectrometer (AMS, Aerodyne Inc.). The gas-phase emissions of NO_x, HC, O_2, CO, and CO_2 were measured undiluted with a gas analyzer emission system (AMA i60, AVL List GmbH). Aerosol sampling for thermal-optical carbon (OC/EC) analysis was performed on undiluted exhaust on quartz filters (Pallflex Tissuequartz, 47 mm).

2.1.2. Aging of the emissions with an oxidation flow reactor (OFR)

The potential secondary aerosol formation upon atmospheric aging was simulated with the potential aerosol mass (PAM) OFR. The reactor consists of a 13 L steel chamber containing two Hg lamps with peak intensities at 185 and 254 nm. In this study only one of the lamps was used and operated at a reduced intensity. The lamp-mounting cylinders were continually purged with N_2 to prevent O_3 and OH formation, and to remove outgassing compounds. The UV light generates ozone and hydroxyl radicals (OH) that oxidize the aerosol as it moves through the chamber. The flow rate through the PAM was controlled to 5–7 L min^{-1}, resulting in an average residence time in the chamber of approximately 113–160 s. It should be noted that different parts of the aerosol experience different residence times since the flow in the reactor was neither a plug flow nor a laminar flow. The same UV light intensity was employed in all the experiments. The humidity of the aerosol prior to entering the reactor is regulated via mixing with a controlled humid air flow, and the water vapor concentration was 0.37 ± 0.02 mol m^{-3}. A continuous injection of CO (40 ppm) was added to the flow to allow calculation of the OH exposure in each experiment. The concentration of CO was measured with a CO/CO_2 analyzer (CO12M, Environment S.A.) while the UV lamps were on ($[CO]_f$) and off ($[CO]_0$). The OH exposure (OH_{exp}) was calculated from the reaction rate constant of CO and OH (k_{OH+CO}), and the CO concentrations by Eq. (1).

$$OH_{exp} = \frac{1}{k_{OH+CO}} \frac{\ln[CO]_0}{\ln[CO]_f} \quad (1)$$

Due to variations in flow rate and OH suppression, the OH exposure varied between experiments (Table S1). The OH exposure (molecules cm^{-3} s) ranged from 3.2×10^{11}–1.3×10^{12}, which represents an atmospheric processing of 2.5–9.9 (4.8 ± 2.6) days if assuming an average OH concentration of 1.5×10^6 molecules cm^{-3} (Mao et al., 2009). However, we observed no dependence on the yield of SOA on OH exposure in this range, which is supported by the literature that shows a low sensitivity of total SOA yields to OH exposure in this range (3–11 days) (Karjalainen et al., 2019).

2.2. Measurement techniques

2.2.1. Effective density

The particle effective density was quantified using the DMA-APM method (McMurry, Wang, Park, & Ehara, 2002). The effective density was measured at four particle mobility diameters: 58.5, 107, 196, and 296 nm. Smaller nucleation mode particles were not measured due to the lower limit of mass detection of the APM (mass detection range: 0.01 to 100 fg). Mobility size (d_p) selection was performed with the DMA after which the APM measured the mass distribution of the selected mobility size by stepping the voltage for a constant rotating speed. The effective density, ρ_{eff}, was derived from the arithmetic mean of the measured APM voltage-number distribution and polystyrene latex (PSL) sphere reference data according to Eq. (2) (McMurry et al., 2002).

$$\rho_{eff} = \rho_{PSL} \frac{V_{APM}}{V_{APM,PSL}} \quad (2)$$

where ρ_{PSL} is the density of the PSL reference particles; V_{APM} is the measured arithmetic mean voltage of the sampled particles for a given mobility size and rpm; and $V_{APM,PSL}$ is the theoretically calculated arithmetic mean voltage of the PSL reference particles for a

given mobility and rpm. Due to potential instrument offsets, the APM was also calibrated by measuring the ρ_{eff} of PSL particles as a function of mobility diameter and comparing the measured density with the PSL manufacturer's specifications (1.05 g cm^{-3}).

2.2.2. Particle size distributions (PSDs)

The particle number size distributions were measured with two scanning mobility particle sizer systems to cover a size range of 3–500 nm. In addition, one particle size bin was measured with the PSM between 1.2 and 3 nm. Particle size distributions (PSDs) in the size range 3–60 nm were measured using the Nano-SMPS that measured close to the engine after an approx. dilution factor of 1:110. Particles size distributions in the size range 11–500 nm were determined with a regular SMPS ('Reg-SMPS') that measured using a dilution factor that varied between 1:500 and 1:900. Particle losses in the thermodenuders were corrected by the particle penetration curve given in Heikkilä et al. (2009), in which the penetration of 3–10 nm particles was 33–68%, and 68–75% for 11–500 nm particles. The PSDs were dilution corrected and the Nano-SMPS concentration was adjusted by comparing the measured particle concentration between 40 and 50 nm where both SMPSs have a good measurement precision. The Nano-SMPS and the Reg-SMPS PSDs were merged by attributing a weighing factor for each size bin in the overlapping size range (11–60 nm), where the Nano-SMPS precision is assumed to decrease with increasing size, and the Reg-SMPS precision to increase with increasing size. The assumed weighing factor ranged from 0 to 100% for each instrument, increasing for the Reg-SMPS (0% at 11 nm increasing up to 100% at 60 nm) and decreasing similarly for the Nano-SMPS with increasing particle size. Two modes, for the nucleation and soot modes, respectively, were fitted to the data by assuming lognormal distributions for each mode. These modes were used to extract the number and mass fractions in each mode from the size distributions.

Mass size distributions were calculated using Eq. (3), utilizing the SMPS data and DMA-APM (section 2.2.1) experimentally determined effective density (ρ_{eff}) as a function of electrical mobility size (d_p).

$$dM \Big/ d\log d_p = \frac{\pi d_p^3}{6} * \rho_{eff}(d_p) * dN \Big/ d\log d_p \tag{3}$$

The effective density of the soot mode particles for all experiments, excluding after aging in the OFR, was assumed to follow a power law function Eq. (4) (Park, Cao, Kittelson, & McMurry, 2003), where C" is a constant and D_{fm} the mass-mobility exponent.

$$\rho_{eff} = C'' d_p^{D_{fm}-3} \tag{4}$$

This was used to extrapolate a power law function for the effective density as a function of particle size of the soot mode. The nucleation mode particles were assumed to be spherical and to mainly originate from the lubricating oil (confirmed by experiments without combustion) and were hence assigned an effective density corresponding to a lubricating oil density of ~0.8 g cm^{-3} (Park, Kittelson, Zachariah, & McMurry, 2004). An example of the effective density and the particle number size distribution fits are shown in Fig. 2. The total mass size distribution is the superposition of the lognormal distribution fits of the mass size distributions of each mode

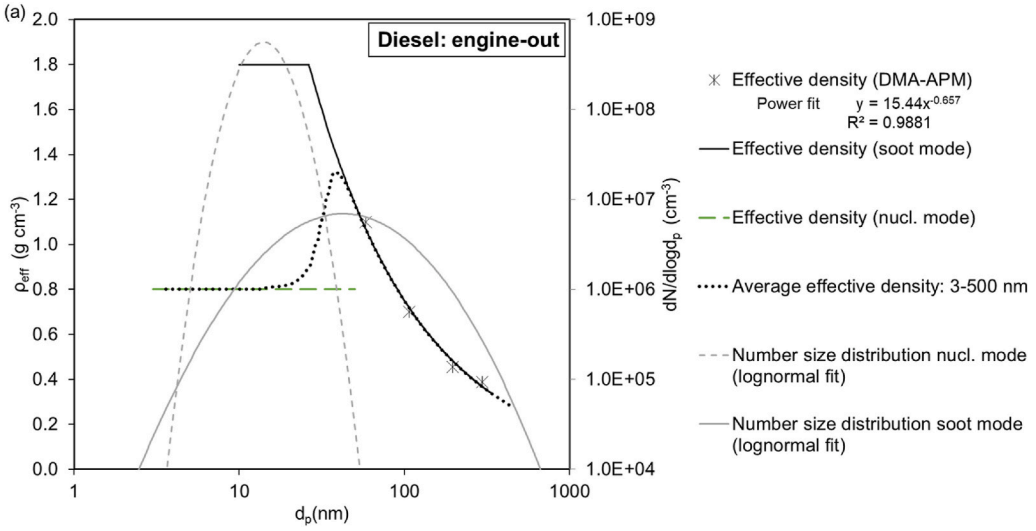

Fig. 2. The effective density of the nucleation and soot mode, together with the respective lognormal mode fits from the particle number size distribution. The effective density was measured at 60, 100, 200 and 300 nm and used for the soot mode. These data were parameterized using a power law fit extrapolated up to 1.8 g cm^{-3} (soot core inherent material density). The effective density is assumed to be 0.8 g cm^{-3} (lubrication oil density) for the nucleation mode, independent of particle size. The average effective density in the particle size range where the nucleation mode and soot mode overlap (for diesel engine-out mainly around 10–50 nm) is based on the fractional contribution of the nucleation mode and soot mode. The effective density below 10 nm is more uncertain; therefore a constant value of 0.8 g cm^{-3} was used for all particles in this size range. The effective density of diesel, HVO and RME, engine-out (fresh and aged) and after the DOC, are shown in Fig. S1.

up to 1000 nm (PM1). The effective density of the particles after the OFR did not follow a power law function. Instead, linear interpolations between each measurement point (d_p: 58.5, 107, 196, and 296 nm) were performed for these experiments. The effective density of particles <60 nm sampled after the OFR were assumed to be pure SOA-derived spherical particles using a constant size independent effective density that was derived from all measurements after the OFR at $d_p = 58.5$ nm ($\rho_{eff} = 1.35 \pm 0.08$ g cm^{-3}). The total mass size distribution after the OFR is estimated from the lognormal distribution fit of the mass size distributions up to 1000 nm (PM1).

The soot mode mass concentrations were assessed from: 1) PM1 from the APM and SMPS (particle mass size distributions), 2) thermal-optically measured elemental carbon (EC) from filters (EUSAAR_2 protocol (Cavalli, Viana, Yttri, Genberg, & Putaud, 2010)), and 3) eBC from the aethalometer. These measurements were compared both for the primary emissions engine-out and emissions downstream of the DOC. The PM1 concentrations derived from the APM-SMPS and EC were in relatively good agreement (EC concentrations accounted for 69% ± 11% of the total soot mode mass). The eBC concentrations using the standard factory settings of the aethalometer yielded values a factor of ~2.8 ± 0.6 higher compared to the EC concentrations that were measured. This factor varied by <25% during repeated measurements (one replicate) of diesel at the engine-out sampling position. The aethalometer eBC concentration was therefore scaled to EC by dividing the original eBC concentrations from the AE33 factory settings by the empirical correction factor 2.8 derived in these experiments.

2.2.3. Chemical composition

The organic aerosol (OA) concentration and chemical composition of the particles were measured using a soot particle aerosol mass spectrometer (Onasch et al., 2012). The data utilized here were recorded in "tungsten only vaporization mode" (referred to as the AMS), that is, the soot module was not engaged. Data analysis was performed using PIKA 1.22A and SQUIRREL 1.62A. Calibration was performed by nebulizing and DMA-selecting 300 nm mobility equivalent diameter ammonium nitrate particles, and comparison of AMS ion rates with particle concentrations measured with a CPC according to standard procedures. OA mass was calculated by applying a standard relative ionization efficiency to nitrate (RIE_{NO3}) of 1.4 (Alfarra et al., 2004) and using the calibrated NO_3 ionization efficiency (IE_{NO3}) of $7.76 \cdot 10^{-8}$ at 132 kHz.

2.3. Emission factors

Emission factors (g per kg burned fuel) were calculated by Eq. (5) that assumes a complete combustion (Gordon et al., 2014; Kirchstetter, Harley, Kreisberg, Stolzenburg, & Hering, 1999) and that all carbon in the fuel was combusted to CO_2.

$$\text{Emission factor (EF)} = 10^3 \frac{\Delta[\text{Pollutant}]}{\Delta[\text{CO}_2]\frac{MW_C}{MW_{CO_2}}} C_f \quad (5)$$

where the concentration of $\Delta[Pollutant]$ and $\Delta[CO_2]$, are in μg/m^3. The $\Delta[CO_2]$ is the difference between the concentration in the exhaust pipe and in the air intake to the combustion cylinder, in order to correct for the increased CO_2 in the exhaust due to the use of EGR. The carbon contents of diesel and RME were analyzed, and the carbon mass fractions (C_f) were 0.85 and 0.772, respectively. The carbon content for HVO was not analyzed; instead it was assumed to have the same mass fraction as diesel (Aatola, Larmi, Sarjovaara, & Mikkonen, 2008).

The emission factors per kg fuel were normalized to the energy content of the fuels and are presented in g/MJ. This was done by dividing the factors by the lower heating values of the fuels (MJ kg fuel^{-1}). The lower heating values are 43.15 MJ kg^{-1} for Swedish ultra-low sulfur diesel, 44.1 MJ kg^{-1} for HVO (Engman et al., 2015), and 37.3 MJ kg^{-1} for RME (Thuijl, Roos, & Beurskens, 2003).

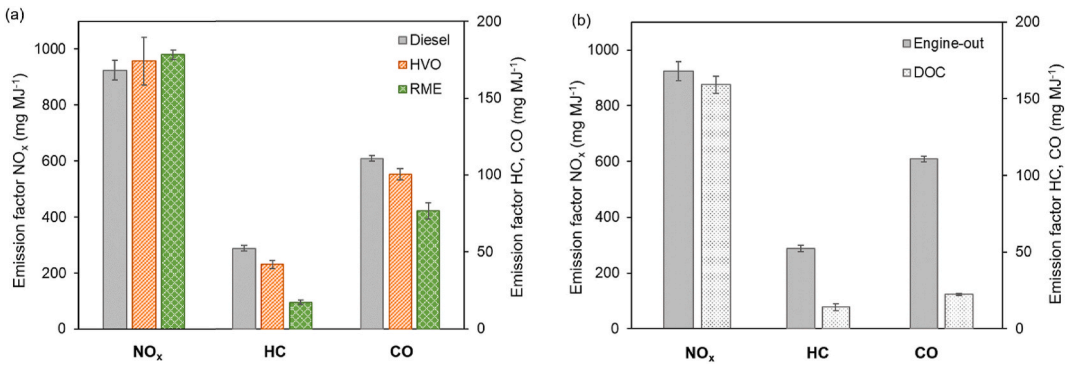

Fig. 3. The emission factors of NO_x (left axis), HC and CO (right axis) for all fuels measured engine-out (a). In (b) the emission factors were compared for engine-out and downstream the DOC for diesel only. The error bars represent ±1 std. dev. of repeated measurements (n = 2–6).

3. Results and discussion

3.1. Primary NO_x, HC, and CO emissions

The effects on NO_x, HC and CO emission factors from substituting petroleum diesel with HVO and RME are presented in Fig. 3a. Substitution with RME had a larger impact on the CO and HC emissions than substitution with HVO. While RME usage reduced the HC and CO emissions by 67% (95% CI [63%, 72%]) and 31% (95% CI [26%, 35%]), respectively, the HVO usage had a lower impact relative to diesel. Substitution with HVO reduced the HC emissions by 20% (95% CI [15%, 25%]) and had a smaller impact on the CO emissions, which were reduced by 9% (95% CI [7%, 12%]) compared to diesel.

Compared to diesel, the small increase in NO_x emissions observed in this study was not statistically significant for neither HVO nor RME (unpaired *t*-test, $p = 0.44$ for HVO, $p = 0.064$ for RME). In this study, the engine was operated with the same ignition delay for all fuels and similar short premixing times. This means that the observed difference in emissions is not due to variations in premixing time due to the different cetane numbers of the tested fuels, which is one important mechanism that can change the emissions for diesel fuels (Giakoumis et al., 2012; Tree & Svensson, 2007).

The decrease in HC and CO emissions were expected and followed previously reported observations of reduced emissions of FAME type biodiesels (Giakoumis, Rakopoulos, Dimaratos, & Rakopoulos, 2012; Horn, Egnell, Johansson, & Andersson, 2007; Georgios Karavalakis et al., 2017) and HVO (George Karavalakis et al., 2016; Kuronen et al., 2007). Most previous studies of FAME type fuels report a slight increase in NO_x emissions (reviewed in Giakoumis et al., 2012; Magín; Lapuerta, Armas, & Rodríguez-Fernández, 2008), while for HVO, both no change (Shukla et al., 2018) and an increase or decrease depending on engine load (George Karavalakis et al., 2016; McCaffery, Karavalakis, Durbin, Jung, & Johnson, 2020; Zubel et al., 2016) have been reported.

The oxygen content of RME can cause a higher oxygen entrainment in the premixing, which would increase the completeness of the combustion and thus decrease the HC and CO emissions (as well as the PM emissions) with a trade-off of slightly higher temperatures

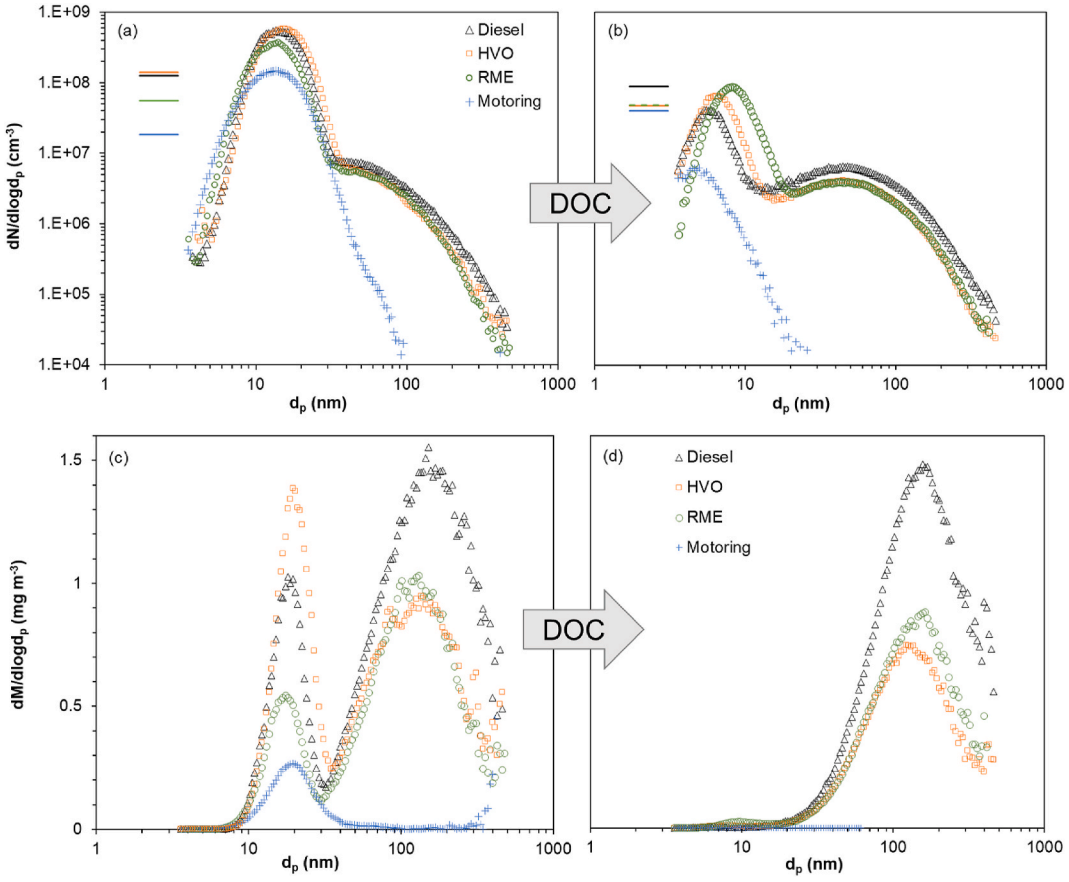

Fig. 4. (a–b) Particle number size distribution, and (c–d) particle mass size distribution of emissions from diesel, HVO, RME combustion, and under motoring conditions before (a, c) and after (b, d) the DOC with Nano-SMPS and Reg-SMPS instruments in a particle size range of 3–500 nm and with the PSM in the range of 1.2–3 nm (one size bin). Note: Motoring was measured after a thermodenuder instead of after the DOC. The mass size distributions were obtained from the superposition of the nucleation and soot mode mass size distributions (Sect. 2.2.2); PSM data not included. The experiment variability of replicates for diesel and HVO can be seen in Fig. S2.

and increased NO_x emissions (M. Lapuerta, Armas, & Rodríguez-Fernández, 2008; Mueller, Boehman, & Martin, 2009). For HVO, the similarities to petroleum diesel in physicochemical properties of the fuel – such as viscosity, lower heating value, heat of vaporization, and stoichiometric air to fuel ratio – are hypothesized to cause similar in-cylinder temperatures as diesel and hence similar NO_x emissions (Shukla et al., 2018). Differences such as higher H/C ratio and the absence of aromatics in HVO compared to diesel are hypothesized to cause the lower HC and CO emissions (McCaffery et al., 2020; Pflaum, Hofmann, Geringer, & Weissel, 2010). The reductions of HC and CO were somewhat lower than previously reported (Bohl, Smallbone, Tian, & Roskilly, 2018; McCaffery et al., 2020; Napolitano et al., 2015; Pflaum et al., 2010), when HVO has been compared to standard diesel with >15% aromatic content. The aromatic content of the Swedish MK1 diesel is <5% which could be the reason for the relatively lower reductions.

The effects of employing the DOC for the case with petroleum diesel are presented in Fig. 3b. The DOC effectively reduced the engine-out HC and CO emission factors by 73% (95% CI [67%, 79%]) and 80% (95% CI [78%, 81%]), respectively. The reduction of HC by the DOC was similar to the reduction caused by a fuel change to RME during engine-out. The DOC had a low influence on the NO_x emissions (5% reduction, 95% CI [0%, 11%]). The DOC converts NO to NO_2, but the individual concentrations of NO and NO_2 were not measured. The conversion to NO_2 can be important as DPFs utilize NO_2 for continuous regeneration (soot removal).

3.2. Primary particle emissions

3.2.1. Particle size distributions

Fig. 4a–d shows the number and mass weighted particle size distributions (3–500 nm) of emissions engine-out and downstream the DOC, as well as for motoring (no combustion). Nanoparticle emissions in the interval 1.2–3 nm particle size (measured with the PSM) are also indicated with horizontal bars. The particle number size distributions were characterized by a nucleation mode and a soot mode, both in the engine-out exhaust (Fig. 4a) and downstream the DOC (Fig. 4b). The emissions during motoring (no combustion) were characterized by a single nucleation mode and no soot mode. Lognormal distributions were fitted to the two modes (SMPS only, example in Fig. S2), and the geometrical mean diameter (GMD), geometrical standard deviation (GSD), and number concentrations for each mode are summarized in Table 1. The DPF reduced particle number emissions by 4 orders of magnitude for all fuels. Because of the high dilution ratio used ($\sim 10^3$), size distributions after the DPF could not be resolved.

Nucleation mode particles were strongly reduced by the DOC for all tested fuels (Table 1). The DOC reduced the nucleation mode particle number concentrations by about one order of magnitude, and the mobility diameters shifted towards smaller sizes compared to the engine-out position (Table 1, Fig. 4a and b). This was also seen in the relatively high concentrations observed by the particle size magnifier (PSM) downstream the DOC compared to the engine-out situation. Similar nucleation mode reductions of diesel exhaust from a light-duty diesel engine was found by Zeraati-Rezaei et al. (2020) who attributed this to decreased concentrations of intermediate and semi-volatile organic compounds. However, their engine was operated with higher EGR which led to a higher soot mode concentration than in this study. Exposing the engine-out aerosol to similar temperatures in the thermodenuders (TDs, 265 °C before the Nano-SMPS and 250 °C before the regular SMPS [Reg-SMPS]) also resulted in substantially reduced nucleation mode number concentrations and sizes for both motoring and combustion (Fig. S3). HVO and RME had a factor 1.2 and 2.3 lower soot mode number concentration, respectively, compared to diesel. The reduction in soot mode mass concentration was a factor 1.6 and 2.3 lower for HVO and RME, respectively, relative to diesel (Table S2). The soot mode GMD was small and similar for all fuels (40–50 nm), and the reduced soot mode number concentration is hence the main cause for the reduced mass emissions for the renewable fuels. The DOC and the TD had only limited effects on the soot mode number concentration, as these particles were mainly composed of thermally stable

Table 1
The particle number concentration and size for all fuels measured engine-out, downstream the DOC, and DOC + DPF. The geometric mean diameter (GMD), geometric standard deviation (GSD), and number emissions (per MJ^{-1}) of the nucleation mode (N*) and soot mode (S*) were estimated from lognormal fits to the bimodal particle number size distributions (example in Fig. S2). The number concentration of the 1.2–3 nm particles was measured by the PSM. The total particle number concentration was calculated from the original SMPS data (3–500 nm). No modes could be fit from the particle size distributions measured downstream the DOC + DPF. The conversion factors for the emissions factors are given.

	Diesel			HVO			RME		
	Engine-out	DOC	DOC + DPF	Engine-out	DOC	DOC + DPF	Engine-out	DOC	DOC + DPF
1.2–3 nm Number concentration (MJ^{-1})	1.05×10^{14}	7.16×10^{13}	2.25×10^{10}	1.13×10^{14}	3.65×10^{13}	1.10×10^{9}	3.47×10^{13}	3.45×10^{13}	1.82×10^{8}
N* GMD (nm)	14.5	6.0		15.7	6.7		13.6	8.3	
N* GSD	1.33	1.26		1.34	1.26		1.35	1.28	
N* Number concentration (MJ^{-1})	3.53×10^{14}	1.96×10^{13}		3.58×10^{14}	3.05×10^{13}		1.76×10^{14}	3.97×10^{13}	
S* GMD (nm)	49.4	48.2		40.4	47.0		49.4	47.0	
S* GSD	2.12	2.12		2.01	2.08		1.92	2.01	
S* Number concentration (MJ^{-1})	1.17×10^{13}	1.04×10^{13}		9.34×10^{12}	6.12×10^{12}		5.07×10^{12}	5.63×10^{12}	
3–500 nm Total number concentration (MJ^{-1})	3.59×10^{14}	3.00×10^{13}	4.12×10^{10}	3.62×10^{14}	3.68×10^{13}	3.17×10^{10}	1.81×10^{14}	4.57×10^{13}	9.00×10^{9}
Emission factor conversion (cm^3 MJ^{-1})	2.01×10^{6}	1.95×10^{6}	1.92×10^{6}	1.91×10^{6}	1.85×10^{6}	1.56×10^{6}	1.47×10^{6}	1.73×10^{6}	1.78×10^{6}

eBC material.

Previous studies on various fuels and diesel engines have indicated that a significant fraction of the nucleation mode of exhaust particles originates from the lubricating oil (de Filippo & Maricq, 2008; Matti Maricq, 2007; Tobias et al., 2001). The lubricants from the moving engine parts have been hypothesized to escape into the combustion chamber with the piston movements and exit with the exhaust emissions. Oil can thus be directly atomized or alternatively, nucleate or condense from oil vapors during cooling and dilution of the exhaust emissions. Together with the similarity in nucleation mode geometric mean diameter (GMD) during motoring and combustion with diesel, HVO, and RME, the results show that the main fraction of the nucleation mode is lubricant derived.

The PSM extends particle size analysis below the detection limit of the Nano-SMPS. The PSM results indicated in Fig. 4a and b suggest that the nucleation mode is broader than could be resolved by the Nano-SMPS. The observation of nonvolatile nanoparticles (down to 1.2 nm) downstream the DOC or TD (Fig. 4b) provide evidence that a significant fraction of the nucleation mode particles had solid or nonvolatile cores onto which more volatile organic material had condensed.

The relationship between particle mobility size and mass was determined with the DMA-APM system and was used in conjunction with the number size distributions to calculate the particle mass size distributions presented in Fig. 4c and d. The effective density decreased with increasing size for all studied particle sizes (d_p = 58.5, 107, 196, 296 nm) (Fig. S1). The mass-mobility exponent, D_{fm} (Eq. (4)), varied between 2.26 and 2.42 for the fuels at engine-out and between 2.33 and 2.41 downstream the DOC. RME had the highest values of D_{fm} and HVO had the lowest values for both sampling positions. Because the nucleation mode was assumed to be dominated by lubricating oil, the material density of the lubricating oil (0.8 g cm^{-3}) was used as the effective density for nucleation mode particles. HVO had the largest nucleation mode mass. The soot mode mass was lower relative to petroleum diesel for both HVO and RME (Fig. 4c). During motoring, no clear soot mode was present and >90% of the mass was in the nucleation mode. The DOC effectively removed the nucleation mode mass (Fig. 4d, Table S2) compared to engine-out for all fuels and during motoring, confirming that the nucleation mode mass was dominated by volatile lubricant-derived particles. The mass GMD of the soot mode was unaffected by the DOC for diesel and HVO but increased from 136.5 nm to 157.1 nm for RME (Table S2).

For all fuels, the measured effective densities of the soot mode downstream the DOC were lower compared to the engine-out (Fig. S1). This indicates that the soot agglomerates became more porous due to the loss of volatile material in the DOC that would otherwise condense onto the soot agglomerates during cooling and dilution. Both the effective density and mass-mobility exponent of particles in the soot mode were slightly higher for RME compared to diesel and HVO. We hypothesize that this was due to differences in the particle morphology. FAME fuels may generate more compact soot aggregates because of stronger soot oxidation that preferentially removes the longest branches from the aggregates. Another explanation could be that the soot agglomerates from RME contain a higher fraction of organic compounds. However, this was contradicted by the measurements of organic aerosol (OA measured with AMS) and eBC presented in the next section.

3.2.2. *Chemical composition and mass emission factors*

As shown by the size distributions, the nonvolatile particle mass emissions were dominated by a soot mode that primarily consists of elemental carbon, which is closely related to the climate relevant black carbon (BC) emissions. Equivalent BC (eBC) was measured continuously with an aethalometer, and eBC emission factors in comparision to diesel were reduced by 48% (95% CI [28%, 69%]) for HVO and 50% (95% CI [26%, 74%]) for RME (Fig. 5). The decrease of eBC emissions observed here is related to the reduced soot mode number concentration (Fig. 4c, Table 1) and is similar to our previous study with higher EGR levels using the same fuels in a similar engine set-up (Gren et al., 2020). Similar eBC reduction potentials have also been reported for HVO by others (Pflaum et al., 2010; Zubel et al., 2016). The driving mechanism for the reduction could be a combination of many parameters. The main hypotheses are: i)

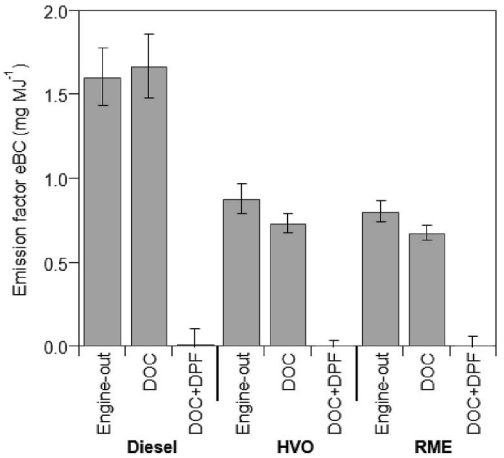

Fig. 5. Equivalent black carbon (eBC) emission factors in mg MJ^{-1} for all tested fuels engine-out, downstream the DOC and downstream the DOC + DPF. Error bars represent ±1 std. dev. The eBC values were divided by the empirically determined correction factor 2.8 to be scaled to EC (Sect. 2.2.2).

the absence of aromatic content which act as soot precursors (McCaffery et al., 2020; Singh, Subramanian, & Singal, 2015; Tan et al., 2013; Wu, Huang, Zhang, Fang, & Yin, 2007), and ii) the more homogenous composition and resulting lower boiling temperature of HVO compared to diesel and RME, which cause improved spray characteristics and mixture formation which reduce the soot formation (Bhardwaj et al., 2014). The eBC reduction for RME is instead likely related to the oxygen content in the RME fuel which has been hypothesized to both increase the completeness of the combustion in local regions of the combustion cylinder and increase the soot oxidation during the late cycle combustion (Magín Lapuerta, Armas, & Rodríguez-Fernández, 2008; Matti Maricq, 2007). The DOC alone had no significant impact on the eBC emission factors, while eBC emissions were almost absent with the addition of the DPF (after the DOC and DPF in combination). We calculated the average eBC removal efficiency after the DPF to 99.4 ± 0.5%. The variability of eBC emission factors was <10% during replicate measurements on diesel (engine-out) and HVO (DOC).

Fig. 6 shows the mass emission factors of equivalent black carbon (eBC), organic aerosol (OA) and the total particle mass calculated from the particle mass size distributions (PM1). The nucleation mode mass fractions of PM1 during engine-out were 18 ± 2% for diesel, 30 ± 3% for HVO, and 18 ± 2% for RME. The DOC reduced the nucleation mode mass fractions to <1% for all fuels. The effect of the DOC on the soot mode mass emission factors was small, with an average reduction of 12 ± 13%. The average eBC concentrations were unaffected by the DOC. We hypothesize that the small mass reduction after the DOC was due primarily to the removal of organic aerosol that was likely (due to the unimodal shape of APM mass distributions) internally mixed with the soot mode eBC rich particles. The effective density of the soot mode was found to decrease after the DOC (Fig. S1). This supports that internally mixed organic components were removed in the DOC, which was confirmed by the OA mass emissions which decreased for all fuels by on average 45 ± 11% after the DOC (Fig. 6). The OA was measured by the AMS, which has a very low collection efficiency of $d_p < 50$ nm; hence, the OA that was measured should primarily originate from the soot mode. The soot mode mass, calculated from the PSDs and the effective densities, correlates reasonably well (by a factor 1.3 higher) with the sum of the measured eBC (scaled to EC by a factor 2.8, Sect. 2.2.3) and OA mass. This also suggests that the OA fraction measured by the AMS captures the organic fraction of the soot mode, but not the organic mass in the nucleation mode.

Looking at the effects of fuel on nucleation mode and OA emissions, we found that HVO emitted the highest nucleation mode mass followed by diesel and RME. For OA measured with the AMS, representing the OA of the soot mode, diesel had the highest emissions followed by HVO and RME. We hypothesize that the difference between diesel and HVO is explained by the higher condensation sink of the soot mode for diesel (Fig. S4), which leads to a higher fraction of the condensable organics ending up in the soot mode. We note that the gas-phase HC emissions were similar for diesel and HVO but three times lower for RME. The results in Fig. 6 show that RME was associated with both lower nucleation mode mass and OA emissions in the soot mode. This suggests that particle phase organic species were significantly reduced for RME compared to the other two fuels in similar fashion as gas-phase HC emissions.

The DOC drastically reduced the nucleation mode mass emissions, but the effect on OA was more modest (average 45% reduction across fuels). We hypothesize that this is because the DOC removes the majority of the condensable mass (Bhardwaj et al., 2014). This in turn leads to a reduction of supersaturations during sampling, thereby suppressing nucleation and early growth by condensation. This results in a much smaller condensation sink provided by the nucleation mode, thus shifting the condensation after the DOC towards the soot mode on a relative basis, explaining the lower effect of the DOC on OA measured by the AMS compared to nucleation mode mass.

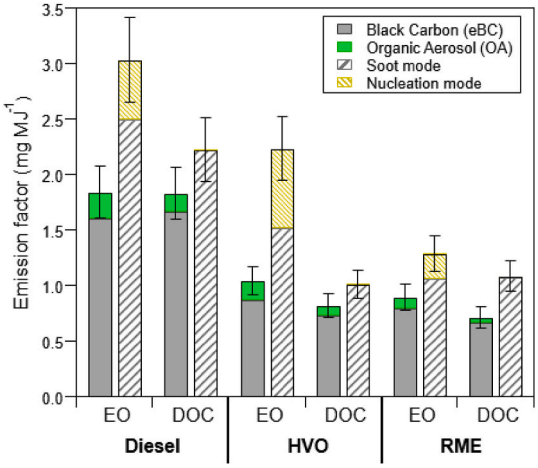

Fig. 6. The mass emission factors of equivalent black carbon (eBC), organic aerosol (OA measured with the AMS), and soot and nucleation modes. The masses of the nucleation and soot mode were derived from particle mass size distributions (Sect. 2.2.2). The error bars show ±1 relative std. dev. of the summed mass of either the eBC and OA, or soot and nucleation modes (PM1), based on replicates of diesel and HVO after the DOC. The eBC values were divided by the empirically determined correction factor 2.8 to be scaled to EC (Sect. 2.2.2).

3.3. Secondary particle emissions

The particle number size distributions and effective densities of the engine-out emissions after simulated atmospheric aging in the OFR are shown in Fig. 7a and b. The shape of the particle size distributions changed upon aging, and a new mode appeared in between the former nucleation and the soot mode (Fig. 7a). After aging, the effective density of the 58.5 nm particles increased to 1.32–1.37 g cm^{-3} regardless of fuel (Fig. 6). This is similar to the literature values of SOA density (Kostenidou et al., 2007; Nakao et al., 2013), indicating that these particles were primarily comprised of SOA. The largest increase in effective density upon aging was for the 107 nm particles which increased from 0.70 to 1.17 g cm^{-3} (HVO), and from 0.73 to 1.13 g cm^{-3} (diesel), respectively (see Fig. 7b). A similar large increase in effective density upon aging at this size was not observed for RME, for which the initial soot mode still dominated at this size. Aged RME emissions instead showed a higher increase in effective density compared to the other fuels at 196 nm. At $d_p > 200$ nm for diesel and HVO (no data on RME), the effective density of the soot mode only increased slightly after aging from the initial values of around 0.4, which is far below the SOA density of ~1.35 g cm^{-3}. The small increase in effective density was attributed to the condensation of only minor fractions of SOA onto the soot mode particles.

The particle mass size distributions engine-out and after the DOC after aging are shown in Fig. 8a and b. The aged PM emissions after the DOC + DPF could not be clearly resolved from the SOA background (Fig. S5c). After aging, the new mode dominated the mass emissions for all fuels engine-out (Fig. 8a) and the bimodality of the particle size distribution was not as clear as before aging. This latter observation is likely due to condensational growth primarily on existing nucleation mode particles. By combining with the DMA-APM observations, we hypothesize that the aged emissions engine-out consist of two particle types: 1) SOA dominated particles that grow due to SOA condensation on existing nucleation mode particle (these particles dominate the mass size distribution) and 2) the soot mode present from the engine-out conditions with only minor fractions of condensed SOA. Notably, the secondary aerosol mass formation was lower compared to diesel for both renewable fuels, with the largest reduction seen for RME as is clearly illustrated in Fig. 8a.

Aging of the exhaust after the DOC had a much lower effect on the mass size distribution (Fig. 8b) compared to aging of engine-out emissions, and only a weak increase similar to the new mode can be seen. Perhaps a larger fraction of the low amounts of formed SOA ended up on the soot mode particles, as the relative surface area of the nucleation mode compared to soot mode particles is lower in this case. We note that these size distributions may not accurately describe real-world aged emissions size distributions since the aging in the reactor speeds up the process and the aerosol dynamics (i.e., physics) may be different compared to the atmosphere.

The mass emission factors of fresh and aged exhaust, estimated from the sum of eBC and OA or mass weighted size distributions (PM1) are shown in Fig. 9a and b. The total aged engine-out PM1 mass emissions were in comparison to the primary emission factors about 5 times higher for diesel, 4 times higher for HVO, and 3 times higher for RME (based on PM1 from the SMPS and effective density derived mass distributions). A strong reduction of aged mass formation of PM1 was observed after the DOC for all fuels. Significant reductions in SOA formation of diesel exhaust after similar aftertreatment systems have been reported in previous studies (Chirico et al., 2010; Karjalainen et al., 2019). Compared to primary emissions, the aged PM1 mass was less than a factor 2 times higher for all fuels downstream the DOC, while the summed aged mass emissions of eBC and OA were even less affected. The eBC + OA consistently showed much lower mass concentrations than the PM1 for the aged emissions engine-out. This may similarly to that described above for the fresh emissions, be due to the reduced collection efficiency of the AMS at particle sizes below 100 nm where most of the aged PM exists.

The total gas-phase HC emissions have been identified as a key parameter in secondary aerosol formation (Karjalainen, Timonen, et al., 2016; Roth et al., 2020). The HC emission factors were significantly lower compared to diesel for RME (67% reduction) and

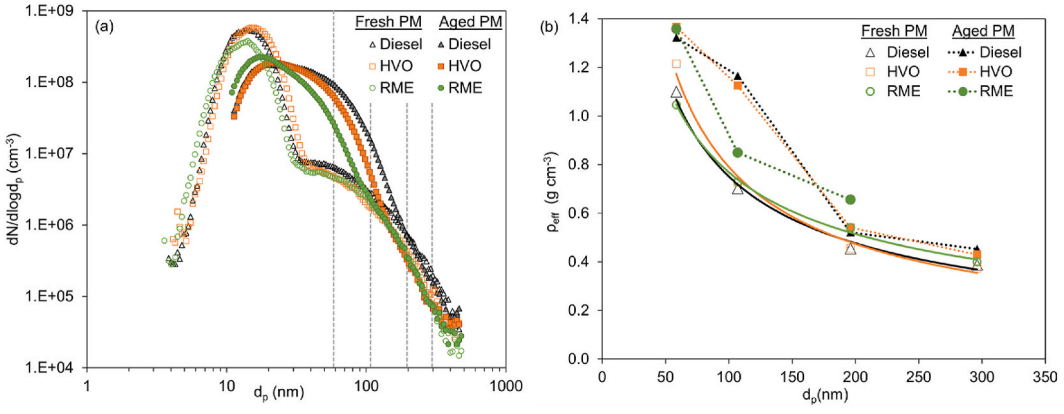

Fig. 7. (a) The particle number size distributions of all fuels engine-out (fresh PM) and after aging in the OFR (aged PM), and (b) corresponding effective densities. The guiding lines in (a) corresponds to the d_p with measured effective density in (b) at d_p 58.5, 107, 196, and 296 nm before and after aging in the OFR. Lines represent the density interpolation used to infer the mass size distribution. The solid lines of the fresh PM were derived from the fitting of a power law function (Park et al., 2003) to the experimental data. The dotted lines are linear interpolations between the experimental data. Extrapolations used to calculate PM1 emissions are shown in Fig. S1.

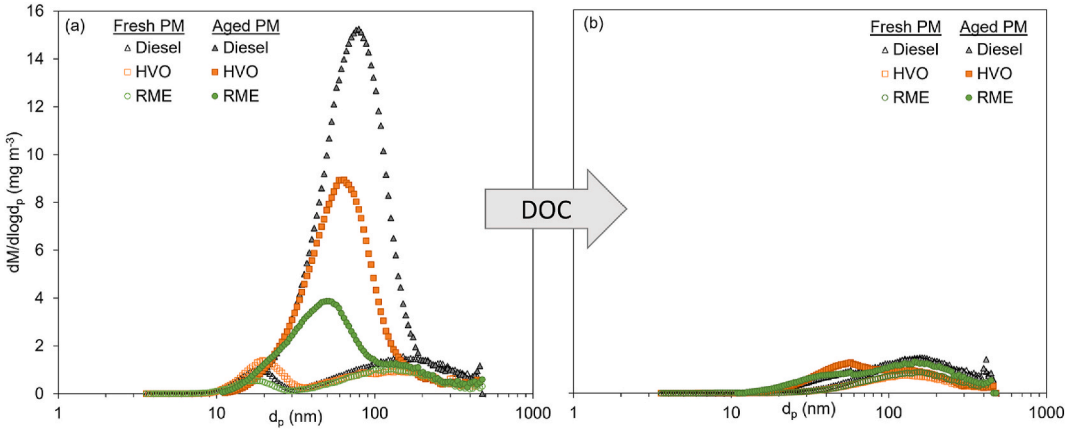

Fig. 8. The particle mass size distributions of diesel, HVO, and RME (fresh PM) and after aging in the OFR (aged PM), engine-out (a) and after the DOC (b). The background in the OFR in comparison to the mass PSDs of aged PM are shown in Fig. S5.

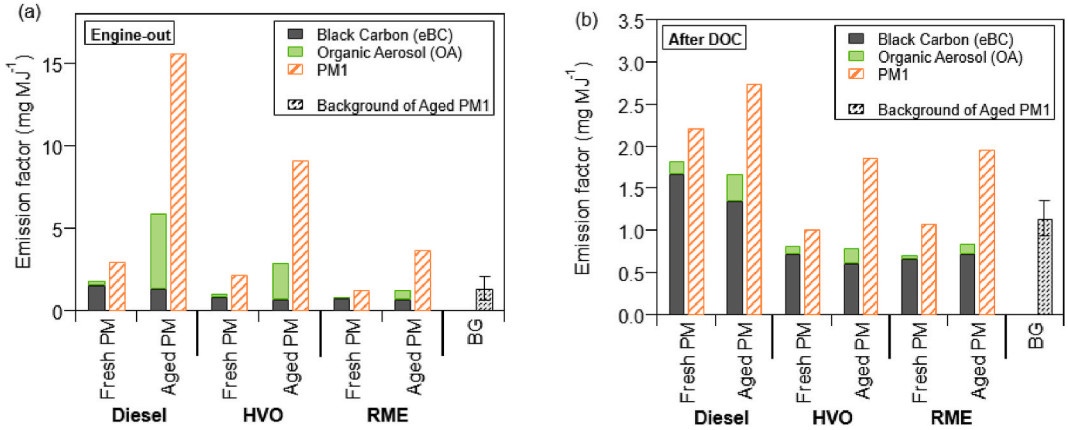

Fig. 9. The mass emission factors of fresh and aged PM: (a) engine-out, and (b) after the DOC. The total mass of aged PM1 represents the upper limit of the possible aged mass estimated from the mass size distributions (Sect. 2.2.2), because the background PM1 formed from impurities may contribute. The mean background contribution of PM1 is shown as a separate bar with error bars of ±1 std. dev. For engine-out, the maximum background of aged mass was 20%, and after the DOC the maximum background contribution was 60%. The eBC values were divided by the empirically determined correction factor 2.8 to be scaled to EC (Sect. 2.2.2).

slightly reduced for HVO (20% reduction) (Fig. 3a). The DOC was found to reduce HC emission by 73% for the diesel combustion (Fig. 3b). In Fig. S6a we show that the HC emissions correlated with aged PM1 mass emissions ($r = 0.96$), supporting that the reduced HC emissions likely explain the lower aged PM emissions. In addition, it has been suggested that the SOA formation of diesel emissions depends on the aromatic content in the fuel (Gentner et al., 2017), and HVO and RME are both aromatic-free fuels. The reduced SOA emissions of RME and HVO compared to diesel may therefore potentially be understood as a combination of reduced HC emissions and aromatic-free fuel. For gasoline engines oxygenated fuels (higher blend of ethanol) have been found to reduce the SOA formation. This was attributed to decreased HC emissions (Roth et al., 2020) and an increased fraction of short-chained organic species (Timonen et al., 2017). In this study the oxygen content of RME caused the decreased HC emissions which we hypothesize is also the main cause of the decreased SOA formation.

The lubricating oil has also been found to influence the secondary aerosol formation independent of fuel in diesel engines (Karjalainen et al., 2019; Le Breton et al., 2019; Watne et al., 2018) The DOC was efficient at removing the nucleation mode particles and hence the lubricant-derived and organic components of the engine-out emissions. This could have further contributed to the reduced secondary PM emission factors (Fig. S6b). However, the effect was likely small in comparison to the fuel-induced effect of altered HC emissions that is illustrated in Fig. S6a.

The emission factors of the total aged PM after the DOC are upper limit values in this study (Fig. 9). By measuring the SOA formation potential of the dilution air, the OFR background contribution could be as high as 60% of the total aged PM mass after the DOC (mass estimated from the mass size distribution of background measurements), while relatively much smaller compared to aged engine-out emissions (20%), see (Fig. S5). Hence, the SOA mass emissions reported after the DOC may be biased high compared to engine-out.

3.4. Limitations

We carried out a detailed study on the fundamental aerosol properties of the exhaust emissions from various exhaust aftertreatment combinations (DOC, DOC + DPF) and fuel choices (diesel, HVO, RME) for a heavy-duty diesel engine operated under low-load ($IMEP_G$ = 6 bar) at steady conditions. The engine was also operated in motored mode to simulate engine breaking. The resulting particle emissions and properties cannot be generalized to all applications of this engine type in real-world use. This study does not cover the effects on aerosol emissions from, for example, variance in engine load and transients in operation, different effective temperatures of the DOC and DPF, specific emissions after engine cold start, or specific DPF regeneration events.

The secondary aerosol formation was simulated with the PAM OFR, which has been shown to yield SOA formation similar to smog chambers when operated under similar conditions. However, both can underestimate the yields compared to the SOA found in the atmosphere (Bruns et al., 2015). Hence, it is not straightforward to estimate the atmospherically relevant absolute SOA mass emissions directly from these observations, since the emissions may be biased low for a number of reasons. SOA yields may be biased low due to wall-losses and SOA precursor fragmentation caused by the intense oxidation in the OFR (Lambe et al., 2015). However, aerosol with high particle surface area entering the OFR, such as in our experiments (2.4–4.0 $\times 10^4$ $\mu m^2\,cm^{-3}$, see Fig. S4), have been found to cause conditions where the wall-losses and fragmentation should be small compared to the mass condensed onto existing particles (Ahlberg, Eriksson, Brune, Roldin, & Svenningsson, 2018). Our measured eBC concentrations were similar before and after aging (Fig. 9), which indicates low particle wall-losses, at least for the soot mode particles. In a similar OFR chamber, particle losses increased from 25% at 50 nm to up to 60% for 10 nm particles at a flow rate of 10 L min^{-1} (Karjalainen, Timonen, et al., 2016). In this study we used a lower flow rate (5–7 L min^{-1}) that may have further increased the losses of small particles. Consequently, absolute number concentrations after aging are not discussed. In addition, parameters such as temperature and relative humidity may significantly influence the SOA yields (e.g. Tillmann et al., 2010; Zhou et al., 2011), and in our oxidation flow reactor, the temperature was relatively high (>28 °C) and the RH relatively low (20–25%), which may have biased the SOA yields further low relative to more typical atmospheric conditions (Tillmann et al., 2010; Zhou et al., 2011). While the absolute emissions are somewhat uncertain, we expect the relative differences in SOA emission factors between the respective fuels to remain robust for a range of atmospheric conditions, since the respective biases are expected to be similar for the different experiments.

4. Conclusions

Renewable diesel fuels and exhaust aftertreatment are used to reduce greenhouse gas emissions and improve air quality by reducing primary emissions. However, for the total atmospheric impact the secondary emissions are also of great importance, which from renewable diesel fuels and from different emission reduction techniques are less known. In line with previous studies, many of which have been reviewed (Knothe, 2010; Knothe et al., 2015; Mahmudul et al., 2017), we found that replacing petroleum diesel with renewable diesel fuels reduced the primary particle emissions and important gas-phase emissions. We found that the engine-out eBC emissions, when normalized to the fuel energy content, were reduced by 48% for HVO and 50% for RME in comparison to petroleum diesel. The reductions in eBC induced by the fuel substitutions were similar after the introduction of the DOC, which was the first in line of the exhaust aftertreatment units included in the study. Engine-out CO and HC emissions were strongly reduced for RME in comparison to both diesel and HVO. The RME reductions in comparison to diesel were 67% (95% CI [63%, 73%]) for HC, and 31% (95% CI [26%, 35%]) for CO. The DOC efficiently reduced the emissions of CO (by 80%), of gas-phase HC (by 73%), and of nucleation mode particles by both number and mass. The DPF additionally reduced eBC and the total PM mass emissions by >99%.

The total mass emissions were estimated using two independent methods: 1) from integrating the SMPS mass weighted size distributions using empirically determined effective densities, and 2) from the sum of eBC and OA (measured by the AMS). The two mass emission estimates were qualitatively in good agreement for the soot mode. The lubricant-originated nucleation mode contributed up to 30% of the total mass, and nonvolatile particles existed down to at least 1.2 nm in particle size. The AMS did not capture the organics in the nucleation mode due to its low collection efficiency of particles below 50 nm (Jayne et al., 2000). The decrease in the particle effective densities after the DOC shows that the organic coating material of soot mode particles was removed in the DOC (increased porosity of the soot agglomerates) for all fuels. The increase in effective densities after aging in the OFR (increasing asymptotically towards the SOA density) indicates that the majority of the SOA condensed on existing nucleation mode particles and to a lesser extent on pre-existing soot mode particles.

Without aftertreatment, the secondary aerosol mass emission factors (per MJ) were 3–5 times higher than the primary emission factors at the engine setting that was investigated. With the DOC, the increase in mass emissions did not exceed a factor 2. It was hypothesized thath the secondary PM yield upon aging in the OFR depended both on the aromatic content of the fuel and the concentration of emitted gas-phase HC. RME generated lower HC emissions and showed a much lower potential secondary PM formation compared to both diesel and HVO. Our results indicate that RME may not only reduce the primary emissions, but also significantly reduce the secondary aerosol mass formation. This is contrary to some previous studies on FAME fuels (Jathar et al., 2017; Watne et al., 2018) that showed slightly increased SOA yields, which calls for further research to improve our understanding of the components that drive the secondary aerosol formation from renewable fuels. The identification of renewable and sustainable fuels that reduce primary emissions and delayed secondary emissions is a particularly important objective to mitigate CO_2 emissions and simultaneously improve air quality with the existing vehicle fleet. This study shows that renewable fuels similar to those examined here can have important potential for reducing both primary and secondary PM emissions in already existing vehicles, especially from those not equipped with aftertreatment systems.

Author contribution

Conceptualization: PK, VBM, JP, MT, LG. Formal data analysis, interpretation and visualization: LG. Engine operation and data analysis: MN, SS. Design of dilution systems, Nano-SMPS and PSM operation and data analysis: LM, PK. Collection of AMS data and interpretation: VBM. AMS data analysis and interpretation: ACE. APM operation and data analysis: JF, TBK. Design of OFR experiments and data analysis: PK, BS. LG prepared the original manuscript, with contributions from VBM and JP. All co-authors have critically reviewed and approved the manuscript.

Declaration of competing interest

The authors declare that they have no known competing financial interests or personal relationships that could have appeared to influence the work reported in this paper.

Acknowledgements

The authors thank Karin Lovén for the OCEC analysis and Fredrik Mattson for initial SMPS and eBC data analysis. Vikram Singh is acknowledged for operating the engine in an initial part of the campaign. The authors thank Kimmo Korhonen for contributions to scientific discussions during the campaign. This research was financed by the Swedish Research Council FORMAS (2016–00697) and AFA Insurance (160323), Sweden. P.K. acknowledges personal funding from Academy of Finland project "EFFi", decision Nr. 322120. T.B. Kristensen acknowledges funding from the Swedish Research Council (Vetenskapsrådet) (2017–05016).

Appendix A. Supplementary data

Supplementary data to this article can be found online at https://doi.org/10.1016/j.jaerosci.2021.105781.

References

Aatola, H., Larmi, M., Sarjovaara, T., & Mikkonen, S. (2008). Hydrotreated vegetable oil (HVO) as a renewable diesel fuel: Trade-off between NOx, particulate emission, and fuel consumption of a heavy duty engine. *SAE International Journal of Engines, 1*(1). https://doi.org/10.4271/2008-01-2500, 2008-01–2500.

Ahlberg, E., Eriksson, A., Brune, W. H., Roldin, P., & Svenningsson, B. (2018). Effect of salt seed particle surface area, composition and phase on secondary organic aerosol mass yields in oxidation flow reactors. *Atmospheric Chemistry and Physics Discussions*, 1–22. https://doi.org/10.5194/acp-2018-1053

Alfarra, M. R., Coe, H., Allan, J. D., Bower, K. N., Boudries, H., Canagaratna, M. R., et al. (2004). Characterization of urban and rural organic particulate in the lower fraser valley using two Aerodyne aerosol mass spectrometers. *Atmospheric Environment, 38*(34), 5745–5758. https://doi.org/10.1016/j.atmosenv.2004.01.054

Amanatidis, S., Ntziachristos, L., Giechaskiel, B., Bergmann, A., & Samaras, Z. (2014). Impact of selective catalytic reduction on exhaust particle formation over excess ammonia events. *Environmental Science and Technology, 48*(19), 11527–11534. https://doi.org/10.1021/es502895v

Bhardwaj, O. P., Lüers, B., Holderbaum, B., Koerfer, T., Pischinger, S., & Honkanen, M. (2014). Utilization of HVO fuel properties in a high efficiency combustion system: Part 2: Relationship of soot characteristics with its oxidation behavior in DPF. *SAE International Journal of Fuels and Lubricants, 7*(3), 979–994. https://doi.org/10.4271/2014-01-2846

Bohl, T., Smallbone, A., Tian, G., & Roskilly, A. P. (2018). Particulate number and NOx trade-off comparisons between HVO and mineral diesel in HD applications. *Fuel, 215*(November 2017), 90–101. https://doi.org/10.1016/j.fuel.2017.11.023

Bruns, E. A., El Haddad, I., Keller, A., Klein, F., Kumar, N. K., Pieber, S. M., et al. (2015). Inter-comparison of laboratory smog chamber and flow reactor systems on organic aerosol yield and composition. *Atmospheric Measurement Techniques, 8*(6), 2315–2332. https://doi.org/10.5194/amt-8-2315-2015

Burtscher, H. (2005). Physical characterization of particulate emissions from diesel engines: A review. *Journal of Aerosol Science, 36*(7), 896–932. https://doi.org/10.1016/j.jaerosci.2004.12.001

Cavalli, F., Viana, M., Yttri, K. E., Genberg, J., & Putaud, J. (2010). *Toward a standardised thermal-optical protocol for measuring atmospheric organic and elemental carbon : The EUSAAR protocol* (pp. 79–89).

Chirico, R., Decarlo, P. F., Heringa, M. F., Tritscher, T., Richter, R., Prévôt, A. S. H., et al. (2010). Impact of aftertreatment devices on primary emissions and secondary organic aerosol formation potential from in-use diesel vehicles: Results from smog chamber experiments. *Atmospheric Chemistry and Physics, 10*(23), 11545–11563. https://doi.org/10.5194/acp-10-11545-2010

Dimitriadis, A., Natsios, I., Dimaratos, A., & Katsaounis, D. (2018). *Evaluation of a hydrotreated vegetable oil (HVO) and effects on emissions of a passenger car diesel engine* (Vol. 4, pp. 1–19). https://doi.org/10.3389/fmech.2018.00007. July 2018.

Drinovec, L., Mocnik, G., Zotter, P., Prévôt, A. S. H., Ruckstuhl, C., Coz, E., et al. (2015). *The " dual-spot " Aethalometer : An improved measurement of aerosol black carbon with real-time loading compensation*. https://doi.org/10.5194/amt-8-1965-2015

Engman, A., Hartikka, T., Honkanen, M., Kiiski, U., Kuronen, M., Lehto, K., et al. (2015). In *Neste renewable diesel handbook*. In Neste, Finland.

de Filippo, A., & Maricq, M. M. (2008). *Diesel Nucleation Mode Particles : Semivolatile or Solid ?* (pp. 7957–7962). https://doi.org/10.1021/es8010332, 42(21).

Gentner, D. R., Jathar, S. H., Gordon, T. D., Bahreini, R., Day, D. A., El Haddad, I., et al. (2017). Review of urban secondary organic aerosol formation from gasoline and diesel motor vehicle emissions. *Environmental Science and Technology, 51*(3), 1074–1093. https://doi.org/10.1021/acs.est.6b04509

Giakoumis, E. G., Rakopoulos, C. D., Dimaratos, A. M., & Rakopoulos, D. C. (2012). Exhaust emissions of diesel engines operating under transient conditions with biodiesel fuel blends. *Progress in Energy and Combustion Science, 38*(5), 691–715. https://doi.org/10.1016/j.pecs.2012.05.002

Gordon, T. D., Presto, A. A., Nguyen, N. T., Robertson, W. H., Na, K., Sahay, K. N., et al. (2014). Secondary organic aerosol production from diesel vehicle exhaust: Impact of aftertreatment, fuel chemistry and driving cycle. *Atmospheric Chemistry and Physics, 14*(9), 4643–4659. https://doi.org/10.5194/acp-14-4643-2014

Gren, L., Malmborg, V. B., Jacobsen, N. R., Shukla, P. C., Bendtsen, K. M., Eriksson, A. C., et al. (2020). Effect of renewable fuels and intake O2 concentration on diesel engine emission characteristics and reactive oxygen species (ROS) formation. *Atmosphere, 11*(6). https://doi.org/10.3390/atmos11060641

Hallquist, M., Wenger, J. C., Baltensperger, U., Rudich, Y., Simpson, D., Claeys, M., Dommen, J., Donahue, N. M., George, C., Goldstein, A. H., Hamilton, J. F., Herrmann, H., Hoffmann, T., Iinuma, Y., Jang, M., Jenkin, M. E., Jimenez, J. L., Kiendler-Scharr, A., Maenhaut, W., … Wildt, J. (2009). The formation, properties and impact of secondary organic aerosol: Current and emerging issues. *Atmospheric Chemistry and Physics, 9*(14), 5155–5236. https://doi.org/10.5194/acp-9-5155-2009

Heikkilä, J., Rönkkö, T., Lähde, T., Lemmetty, M., Arffman, A., Virtanen, A., et al. (2009). Effect of open channel filter on particle emissions of modern diesel engine. *Journal of the Air and Waste Management Association, 59*(10), 1148–1154. https://doi.org/10.3155/1047-3289.59.10.1148

Horn, U., Egnell, R., Johansson, B., & Andersson, Ö. (2007). Detailed heat release analyses with regard to combustion of RME and oxygenated fuels in an HSDI diesel engine. *SAE Technical Papers, 116*, 464–482. https://doi.org/10.4271/2007-01-0627, 2007.

Jathar, S. H., Friedman, B., Galang, A. A., Link, M. F., Brophy, P., Volckens, J., et al. (2017). Linking load, fuel, and emission controls to photochemical production of secondary organic aerosol from a diesel engine. *Environmental Science and Technology, 51*(3), 1377–1386. https://doi.org/10.1021/acs.est.6b04602

Jayne, J. T., Leard, D. C., Zhang, X., Davidovits, P., Smith, K. A., Kolb, C. E., et al. (2000). Development of an aerosol mass spectrometer for size and composition analysis of submicron particles. *Aerosol Science and Technology, 33*(1–2), 49–70. https://doi.org/10.1080/027868200410840

Karavalakis, G., Gysel, N., Schmitz, D. A., Cho, A. K., Sioutas, C., Schauer, J. J., et al. (2017). Impact of biodiesel on regulated and unregulated emissions, and redox and proinflammatory properties of PM emitted from heavy-duty vehicles. *The Science of the Total Environment*, 1230–1238. https://doi.org/10.1016/j.scitotenv.2017.01.187, 584–585.

Karavalakis, G., Jiang, Y., Yang, J., Durbin, T., Nuottimäki, J., & Lehto, K. (2016). Emissions and fuel economy evaluation from two current technology heavy-duty trucks operated on HVO and FAME blends. *SAE International Journal of Fuels and Lubricants, 9*(1), 177–190. https://doi.org/10.4271/2016-01-0876

Karjalainen, P., Ntziachristos, L., Murtonen, T., Wihersaari, H., Simonen, P., Mylläri, F., et al. (2016). Heavy duty diesel exhaust particles during engine motoring formed by lube oil consumption. *Environmental Science and Technology, 50*(22), 12504–12511. https://doi.org/10.1021/acs.est.6b03284

Karjalainen, P., Rönkkö, T., Pirjola, L., Heikkilä, J., Happonen, M., Arnold, F., et al. (2014). Sulfur driven nucleation mode formation in diesel exhaust under transient driving conditions. *Environmental Science and Technology, 48*(4), 2336–2343. https://doi.org/10.1021/es405009g

Karjalainen, P., Rönkkö, T., Simonen, P., Ntziachristos, L., Juuti, P., Timonen, H., et al. (2019). Strategies to diminish the emissions of particles and secondary aerosol formation from diesel engines. *Environmental Science and Technology, 53*(17), 10408–10416. https://doi.org/10.1021/acs.est.9b04073

Karjalainen, P., Timonen, H., Saukko, E., Kuuluvainen, H., Saarikoski, S., Aakko-Saksa, P., et al. (2016). Time-resolved characterization of primary particle emissions and secondary particle formation from a modern gasoline passenger car. *Atmospheric Chemistry and Physics, 16*(13), 8559–8570. https://doi.org/10.5194/acp-16-8559-2016

Kirchstetter, T. W., Harley, R. A., Kreisberg, N. M., Stolzenburg, M. R., & Hering, S. V. (1999). On-road measurement of fine particle and nitrogen oxide emissions from light- and heavy-duty motor vehicles. *Atmospheric Environment, 33*(18), 2955–2968. https://doi.org/10.1016/S1352-2310(99)00089-8

Kittelson, D. B. (1998). Engines and nanoparticles: A review. *Journal of Aerosol Science, 29*(5–6), 575–588. https://doi.org/10.1016/S0021-8502(97)10037-4

Knothe, G. (2010). Biodiesel and renewable diesel: A comparison. *Progress in Energy and Combustion Science, 36*(3), 364–373. https://doi.org/10.1016/j.pecs.2009.11.004

Knothe, G., Krahl, J., & Van Gerpen, J. (2015). *The biodiesel handbook*. Elsevier.

Kostenidou, E., Pathak, R. K., Pandis, S. N., Kostenidou, E., Pathak, R. K., An, S. N. P., et al. (2007). *An algorithm for the calculation of secondary organic aerosol density combining AMS and SMPS data an algorithm for the calculation of secondary organic aerosol density combining AMS and SMPS data*. https://doi.org/10.1080/02786820701666270

Kuronen, M., Mikkonen, S., Aakko, P., & Murtonen, T. (2007). *Hydrotreated vegetable oil as fuel for heavy duty diesel engines* (Vol. 724). https://doi.org/10.4271/2007-01-4031

Kuuluvainen, H., Karjalainen, P., Saukko, E., Ovaska, T., Sirviö, K., Honkanen, M., et al. (2020). Nonvolatile ultrafine particles observed to form trimodal size distributions in non-road diesel engine exhaust. *Aerosol Science and Technology*, 1–14. https://doi.org/10.1080/02786826.2020.1783432, 0(0).

Lambe, A. T., Chhabra, P. S., Onasch, T. B., Brune, W. H., Hunter, J. F., Kroll, J. H., et al. (2015). Effect of oxidant concentration, exposure time, and seed particles on secondary organic aerosol chemical composition and yield. *Atmospheric Chemistry and Physics, 15*(6), 3063–3075. https://doi.org/10.5194/acp-15-3063-2015

Lapuerta, M., Armas, O., & Rodríguez-Fernández, J. (2008). Effect of biodiesel fuels on diesel engine emissions. *Progress in Energy and Combustion Science, 34*(2), 198–223. https://doi.org/10.1016/j.pecs.2007.07.001

Le Breton, M., Psichoudaki, M., Hallquist, M., Watne, K., Lutz, A., & Hallquist, M. (2019). Application of a FIGAERO ToF CIMS for on-line characterization of real-world fresh and aged particle emissions from buses. *Aerosol Science and Technology, 53*(3), 244–259. https://doi.org/10.1080/02786826.2019.1566592

Liu, Z. G., Eckerle, W. A., & Ottinger, N. A. (2018). Gas-phase and semivolatile organic emissions from a modern nonroad diesel engine equipped with advanced aftertreatment. *Journal of the Air and Waste Management Association, 68*(12), 1333–1345. https://doi.org/10.1080/10962247.2018.1505676

Mahmudul, H. M., Hagos, F. Y., Mamat, R., Adam, A. A., Ishak, W. F. W., & Alenezi, R. (2017). Production , characterization and performance of biodiesel as an alternative fuel in diesel engines – a review. *Renewable and Sustainable Energy Reviews, 72*(April 2016), 497–509. https://doi.org/10.1016/j.rser.2017.01.001

Malmborg, V. B., Eriksson, A. C., Shen, M., Nilsson, P., Gallo, Y., Waldheim, B., et al. (2017). *Evolution of in-cylinder diesel engine soot and emission characteristics investigated with on-line aerosol mass spectrometry*. Environmental Science & Technology. https://doi.org/10.1021/acs.est.6b03391

Mamakos, A., Schwelberger, M., Fierz, M., & Giechaskiel, B. (2019). Effect of selective catalytic reduction on exhaust nonvolatile particle emissions of Euro VI heavy-duty compression ignition vehicles. *Aerosol Science and Technology, 53*(8), 898–910. https://doi.org/10.1080/02786826.2019.1610153

Mao, J., Ren, X., Brune, W. H., Olson, J. R., Crawford, J. H., Fried, A., et al. (2009). Airborne measurement of OH reactivity during INTEX-B. *Atmospheric Chemistry and Physics, 9*(1), 163–173. https://doi.org/10.5194/acp-9-163-2009

Matti Maricq, M. (2007). Chemical characterization of particulate emissions from diesel engines: A review. *Journal of Aerosol Science, 38*(11), 1079–1118. https://doi.org/10.1016/j.jaerosci.2007.08.001

McCaffery, C., Karavalakis, G., Durbin, T., Jung, H., & Johnson, K. (2020). Engine-out emissions characteristics of a light duty vehicle operating on a hydrogenated vegetable oil renewable diesel. *SAE Technical Papers*, 1–11. https://doi.org/10.4271/2020-01-0337, 2020-April(April).

McMurry, P. H., Wang, X., Park, K., & Ehara, K. (2002). The relationship between mass and mobility for atmospheric particles: A new technique for measuring particle density. *Aerosol Science and Technology, 36*(2), 227–238. https://doi.org/10.1080/027868202753504083

Mizushima, N., Kawano, D., Ishii, H., Takada, Y., & Sato, S. (2014). Evaluation of real- world emissions from heavy-duty diesel vehicle fueled with FAME, HVO and BTL using PEMS. *SAE technical papers*. https://doi.org/10.4271/2014-01-2823, 2014-Octob.

Mueller, C. J., Boehman, A. L., & Martin, G. C. (2009). An experimental investigation of the origin of increased NOx emissions when fueling a heavy-duty compression-ignition engine with soy biodiesel. *SAE International Journal of Fuels and Lubricants, 2*(1), 789–816. https://doi.org/10.4271/2009-01-1792

Murtonen, T., Aakko-Saksa, P., Kuronen, M., Mikkonen, S., & Lehtoranta, K. (2010). Emissions with heavy-duty diesel engines and vehicles using FAME, HVO and GTL fuels with and without DOC+ POC aftertreatment. *SAE International Journal of Fuels and Lubricants, 2*(2), 147–166.

Na, K., Biswas, S., Robertson, W., Sahay, K., Okamoto, R., Mitchell, A., et al. (2015). Impact of biodiesel and renewable diesel on emissions of regulated pollutants and greenhouse gases on a 2000 heavy duty diesel truck. *Atmospheric Environment, 107*(x), 307–314. https://doi.org/10.1016/j.atmosenv.2015.02.054

Nakao, S., Tang, P., Tang, X., Clark, C. H., Qi, L., Seo, E., et al. (2013). *Density and elemental ratios of secondary organic aerosol : Application of a density prediction method. 68* pp. 273–277). https://doi.org/10.1016/j.atmosenv.2012.11.006

Napolitano, P., Beatrice, C., Guido, C., Del Giacomo, N., Pellegrini, L., & Scorletti, P. (2015). Hydrocracked fossil oil and hydrotreated vegetable oil (HVO) effects on combustion and emissions performance of "torque-controlled" diesel engines. *SAE Technical Papers*. https://doi.org/10.4271/2015-24-2497

Ntziachristos, L., Giechaskiel, B., Pistikopoulos, P., Samaras, Z., Mathis, U., Mohr, M., et al. (2004). Performance evaluation of a novel sampling and measurement system for exhaust particle characterization. *SAE Technical Papers*, (724), 2004. https://doi.org/10.4271/2004-01-1439

Onasch, T. B., Trimborn, A., Fortner, E. C., Jayne, J. T., Kok, G. L., Davidovits, P., et al. (2012). *Soot particle aerosol mass Spectrometer : Development , validation , and initial application soot particle aerosol mass Spectrometer*. Development. https://doi.org/10.1080/02786826.2012.663948. Validation , and Initial Application. 6826.

Park, K., Cao, F., Kittelson, D. B., & McMurry, P. H. (2003). Relationship between particle mass and mobility for diesel exhaust particles. *Environmental Science and Technology, 37*(3), 577–583. https://doi.org/10.1021/es025960v

Park, K., Kittelson, D. B., Zachariah, M. R., & McMurry, P. H. (2004). Measurement of inherent material density of nanoparticle agglomerates. *Journal of Nanoparticle Research, 6*(2/3), 267–272. https://doi.org/10.1023/b:nano.0000034657.71309.e6

Pflaum, H., Hofmann, P., Geringer, B., & Weissel, W. (2010). Potential of hydrogenated vegetable oil (HVO) in a modern diesel engine. SAE Technical Papers https://doi.org/10.4271/2010-32-0081.

Popovicheva, O. B., Irimiea, C., Carpentier, Y., Ortega, I. K., Kireeva, E. D., Shonija, N. K., et al. (2017). Chemical composition of diesel/biodiesel particulate exhaust by FTIR spectroscopy and mass spectrometry: Impact of fuel and driving cycle. *Aerosol and Air Quality Research, 17*(7), 1717–1734. https://doi.org/10.4209/aaqr.2017.04.0127

Pourkhesalian, A. M., Stevanovic, S., Rahman, M. M., Faghihi, E. M., Bottle, S. E., Masri, A. R., et al. (2015). Effect of atmospheric aging on volatility and reactive oxygen species of biodiesel exhaust nano-particles. *Atmospheric Chemistry and Physics, 15*(16), 9099–9108. https://doi.org/10.5194/acp-15-9099-2015

Pourkhesalian, A. M., Stevanovic, S., Salimi, F., Rahman, M. M., Wang, H., Pham, P. X., et al. (2014). Influence of fuel molecular structure on the volatility and oxidative potential of biodiesel particulate matter. *Environmental Science and Technology, 48*(21), 12577–12585. https://doi.org/10.1021/es503160m

Reşitoğlu, I. A., Altinişik, K., & Keskin, A. (2015). The pollutant emissions from diesel-engine vehicles and exhaust aftertreatment systems. *Clean Technologies and Environmental Policy, 17*(1), 15–27. https://doi.org/10.1007/s10098-014-0793-9

Robinson, A. L., Donahue, N. M., Shrivastava, M. K., Weitkamp, E. A., Sage, A. M., Grieshop, A. P., et al. (2007). Rethinking organic aerosols: Semivolatile emissions and photochemical aging. *315*(March), 1259–1263.

Rönkkö, T., Lähde, T., Heikkilä, J., Pirjola, L., Bauschke, U., Arnold, F., et al. (2013). Effects of gaseous sulphuric acid on diesel exhaust nanoparticle formation and characteristics. *Environmental Science and Technology, 47*(20), 11882–11889. https://doi.org/10.1021/es402354y

Rönkkö, T., Virtanen, A., Vaaraslahti, K., Keskinen, J., Pirjola, L., & Lappi, M. (2006). Effect of dilution conditions and driving parameters on nucleation mode particles in diesel exhaust : Laboratory and on-road study. *Atmospheric Environment, 40*, 2893–2901. https://doi.org/10.1016/j.atmosenv.2006.01.002

Roth, P., Yang, J., Peng, W., Cocker, D. R., Durbin, T. D., Asa-Awuku, A., et al. (2020). Intermediate and high ethanol blends reduce secondary organic aerosol formation from gasoline direct injection vehicles. *Atmospheric Environment, 220*(May 2019), 117064. https://doi.org/10.1016/j.atmosenv.2019.117064

Savic, N., Rahman, M. M., Miljevic, B., Saathoff, H., Naumann, K. H., Leisner, T., et al. (2016). Influence of biodiesel fuel composition on the morphology and microstructure of particles emitted from diesel engines. *Carbon*. https://doi.org/10.1016/j.carbon.2016.03.061

Schauer, J. J., Fraser, M. P., Cass, G. R., & Simoneit, B. R. T. (2002). Source reconciliation of atmospheric gas-phase and particle-phase pollutants during a severe photochemical smog episode. *Environmental Science and Technology, 36*(17), 3806–3814. https://doi.org/10.1021/es011458j

Shukla, P. C., Shamun, S., Gren, L., Malmborg, V., Pagels, J., & Tuner, M. (2018). Investigation of particle number emission characteristics in a heavy-duty compression ignition engine fueled with hydrotreated vegetable oil (HVO). *SAE International Journal of Fuels and Lubricants, 11*(4), 495–505. https://doi.org/10.4271/2018-01-0909

Singh, D., Subramanian, K. A., & Singal, S. K. (2015). Emissions and fuel consumption characteristics of a heavy duty diesel engine fueled with Hydroprocessed Renewable Diesel and Biodiesel. *Applied Energy, 155*(April 2003), 440–446. https://doi.org/10.1016/j.apenergy.2015.06.020

Sorathia, H. S., Rahhod, P. P., Sorathiya, A. S., Engineering, M., College, G. E., & Kutch, B. (2012). Effect of exhaust gas recirculation (EGR) on NOx emission C . I . engine - a review study. *Ijaers, 1*(3), 223–227.

Surawski, N., Miljevic, B., Ayoko, G. A., Eltahir, S., Stevanovic, S., Fairfull-Smith, K. E., et al. (2011). A physico-chemical characterisation of particulate emissions from a compression ignition engine: The influence of biodiesel feedstock. *Environmental Science & Technology, 45*, 10337–10343. https://doi.org/10.1021/es2018797

Tan, C., Xu, H., Shuai, S. J., Ghafourian, A., Liu, D., & Tian, J. (2013). Investigation on transient emissions of a turbocharged diesel engine fuelled by HVO blends. *SAE International Journal of Engines, 6*(2), 1046–1058. https://doi.org/10.4271/2013-01-1307

Thuijl, E. Van, Roos, C., & Beurskens, L. (2003). *An overview of biofuel technologies, markets and policies in Europe. January*, 1–64 http://www.ssc.it/pdf/2005/biofuel_UE2005.pdf.

Tillmann, R., Hallquist, M., Jonsson, Å. M., Kiendler-Scharr, A., Saathoff, H., Iinuma, Y., et al. (2010). Influence of relative humidity and temperature on the production of pinonaldehyde and OH radicals from the ozonolysis of α-pinene. *Atmospheric Chemistry and Physics, 10*(15), 7057–7072. https://doi.org/10.5194/acp-10-7057-2010

Timonen, H., Karjalainen, P., Saukko, E., Saarikoski, S., Aakko-Saksa, P., Simonen, P., et al. (2017). Influence of fuel ethanol content on primary emissions and secondary aerosol formation potential for a modern flex-fuel gasoline vehicle. *Atmospheric Chemistry and Physics, 17*(8), 5311–5329. https://doi.org/10.5194/acp-17-5311-2017

Tobias, H. J., Beving, D. E., Mcmurry, P. H., Zarling, D., Waytulonis, R., & Kittelson, D. B. (2001). Chemical analysis of diesel engine nanoparticles using a nano-DMA/thermal desorption. *Particle Beam Mass Spectrometer, 35*(11), 2233–2243. https://doi.org/10.1021/es0016654

Tree, D. R., & Svensson, K. I. (2007). Soot processes in compression ignition engines. *Progress in Energy and Combustion Science, 33*(3), 272–309. https://doi.org/10.1016/j.pecs.2006.03.002

Watne, Å. K., Psichoudaki, M., Ljungström, E., Le Breton, M., Hallquist, M., Jerksjö, M., et al. (2018). Fresh and oxidized emissions from in-use transit buses running on diesel, biodiesel, and CNG. *Environmental Science and Technology, 52*(14), 7720–7728. https://doi.org/10.1021/acs.est.8b01394

Wu, T., Huang, Z., Zhang, W. G., Fang, J. H., & Yin, Q. (2007). Physical and chemical properties of GTL - diesel fuel blends and their effects on performance and emissions of a multicylinder DI compression ignition engine. *Energy & Fuels, 21*(4), 1908–1914. https://doi.org/10.1021/ef0606512

Zeraati-Rezaei, S., Alam, M. S., Xu, H., Beddows, D. C., & Harrison, R. M. (2020). Size-resolved physico-chemical characterization of diesel exhaust particles and efficiency of exhaust aftertreatment. *Atmospheric Environment, 222*(October 2019), 117021. https://doi.org/10.1016/j.atmosenv.2019.117021

Zheng, M., Reader, G. T., & Hawley, J. G. (2004). Diesel engine exhaust gas recirculation - a review on advanced and novel concepts. *Energy Conversion and Management, 45*(6), 883–900. https://doi.org/10.1016/S0196-8904(03)00194-8

Zhou, J., Elser, M., Huang, R.-J., Krapf, M., Fröhlich, R., Bhattu, D., Stefenelli, G., Zotter, P., Bruns, E. A., Pieber, S., Ni, H., Wang, Q., Wang, Y., Zhou, Y., Chen, C., Xiao, M., Slowik, J. G., Brown, S., Cassagnes, L.-E., … Dommen, J. (2019). Predominance of secondary organic aerosol to particle-bound reactive oxygen species activity in fine ambient aerosol. *Atmospheric Chemistry and Physics Discussions*, (April), 1–26. https://doi.org/10.5194/acp-2019-190

Zhou, Y., Zhang, H., Parikh, H. M., Chen, E. H., Rattanavaraha, W., Rosen, E. P., et al. (2011). Secondary organic aerosol formation from xylenes and mixtures of toluene and xylenes in an atmospheric urban hydrocarbon mixture: Water and particle seed effects (II). *Atmospheric Environment, 45*(23), 3882–3890. https://doi.org/10.1016/j.atmosenv.2010.12.048

Zubel, M., Bhardwaj, O. P., Heuser, B., Holderbaum, B., Doerr, S., & Nuottimäki, J. (2016). Advanced fuel formulation approach using blends of paraffinic and oxygenated biofuels: Analysis of emission reduction potential in a high efficiency diesel combustion system. *SAE Int. J. Fuels Lubr., 9*(3), 481–492. https://doi.org/10.4271/2016-01-2179